Brainwide mesoscale functional networks revealed by focal infrared neural stimulation of the amygdala

An Ping[1,2], Jianbao Wang[1,2,4], Miguel Ángel García-Cabezas[6], Lihui Li[1,3], Jianmin Zhang[1], Junming Zhu*[1], Katalin M. Gothard[5]*, Anna Wang Roe[1,2,3,4]*

Affiliations:

[1] Department of Neurosurgery of the Second Affiliated Hospital and Interdisciplinary Institute of Neuroscience and Technology, School of Medicine, Zhejiang University, Hangzhou, China

[2] MOE, School of Medicine, Zhejiang University, Hangzhou, China

[3] Key Laboratory for Biomedical Engineering of Ministry of Education, College of Biomedical Engineering and Instrument Science, Zhejiang University, Hangzhou, China

[4] MOE Frontier Science Center for Brain Science and Brain-machine Integration, Zhejiang University, Hangzhou, China

[5] Departments of Physiology and Neuroscience, University of Arizona, Tucson, USA

[6] Department of Anatomy, Histology, and Neuroscience, School of Medicine, Autónoma University of Madrid, Madrid, Spain

*Corresponding author. Email: annawang@zju.edu.cn

Summary: The primate amygdala serves to evaluate emotional content of sensory inputs and modulate emotional and social behaviors; prefrontal, multisensory and autonomic aspects of these circuits are mediated predominantly via the basal (BA), lateral (LA), and central (CeA) nuclei, respectively. Based on recent electrophysiological evidence suggesting mesoscale (millimeters-scale) nature of intra-amygdala functional organization, we have investigated the connectivity of these nuclei using infrared neural stimulation (INS) of single mesoscale sites coupled with mapping in ultrahigh field 7T functional magnetic resonance imaging (fMRI), namely INS-fMRI. Following stimulation of multiple sites within amygdala of single individuals, a 'mesoscale functional connectome' of amygdala connectivity (of BA, LA, and CeA) was obtained. This revealed the mesoscale nature of connected sites, the spatial patterns of functional connectivity, and the topographic relationships (parallel, sequential, or interdigitating) of nucleus-specific connections. These findings provide novel perspectives on the brainwide circuits modulated by the amygdala.

Key words: Infrared neural stimulation, Amygdala, Ultrahigh field fMRI, Brainwide network, Mesoscale topography, Connectional topography, Intra-individual datasets, Mesoscale connectome

1. Introduction

The mammalian amygdala evaluates the emotional salience of inputs from all sensory modalities and contributes to the elaboration of emotional and social behaviors in response to stimuli of significance (Adolphs and Anderson, 2018; LeDoux, 2007). This brainwide coordination by the amygdala is achieved by integrating and disseminating neural information across sensory-motor and decision networks (Bickart et al., 2014; Gothard, 2020; Janak and Tye, 2015). Closer evaluation, using local field potential and current source density recordings in Macaque amygdala, has revealed a clear mesoscale (millimeters-scale) signature of intra-amygdala function/circuitry (McHale et al., 2022; Morrow et al., 2019). This raises the exciting possibility that connectional relationships between the amygdala and brainwide networks is also organized at mesoscale.

The amygdala contains multiple subdivisions, of which we focus on the Basal (BA), Lateral (LA), and Central (CeA) nuclei, known to mediate predominantly prefrontal, multisensory, and autonomic regulatory circuits, respectively (Amaral and Price, 1984; Medina et al., 2023; Pessoa et al., 2019; Puelles, 2001; Swanson and Petrovich, 1998). Previous studies have shown that the connectivity of these nuclei is quite heterogeneous, appropriate for supporting a broad spectrum of behavioral axes (Klein-Flügge et al., 2022; Scangos et al., 2021). Not only does each nucleus have distinctive cell types and cell densities (Yu et al., 2023), even single neurons within a subdivision of the amygdala exhibit distinct targeting patterns, projecting to either 1, 2, 3, or 4 cortical sites (Zeisler et al., 2023). Electrical stimulation of nuclear-specific targets in the human amygdala combined with neuroimaging revealed the existence of multiple distinct networks and a reproducible temporal pattern of activation (Sawada et al., 2022). Functional multi-site electrophysiological current source density recordings show that this diversity results in distinct (e.g. visual, tactile, and auditory) mesoscale functional organization within the amygdala in behaving monkeys (McHale et al., 2022; Morrow et al., 2019). Thus, existing studies point to heterogeneous yet functionally specific connection patterns that may vary within each nucleus, motivating further study of amygdala-related brainwide functional circuits at mesoscale.

Here, to establish an understanding of network architecture between the amygdala and cortical networks at mesoscale, we apply a novel method termed Infrared neural stimulation (INS) combined with high-resolution functional magnetic resonance imaging (fMRI), namely INS-fMRI (Xu et al., 2019). This non-viral method maps the functional connectivity between anatomically localized, mesoscale nodes in the primate amygdala and numerous cortical areas. Specifically, brief (0.25msec) pulses of infrared (1875nm wavelength) light delivered (via 200um optical fiber) in pulse trains (200hz, duration 0.5sec) stimulate submillimeter clusters of neurons, leading to specific activation of connected sites whose locations are mapped at brainwide scale by recording Blood Oxygen Level Dependent (BOLD) signals (for review of INS, see (Chernov and Roe, 2014; Goyal et al., 2012; Thompson, 2014); for membrane capacitance effects see (Shapiro et al., 2012) ; for safety and damage thresholds in primates, see (Chernov et al., 2014; Pan et al., 2023)). As INS reveals functional connectivity, extending two synapses from the stimulation site (Xu et al., 2019), it evokes brainwide activations that prove to be highly anatomically and functionally specific (Shi et al., 2021; Yao et al., 2023). INS thus

provides distinct benefits for high resolution brainwide circuit mapping compared with other electrical, optogenetic, and anatomical tracing methods (Klink et al., 2017; Roe et al., 2015). One important advantage of this approach is that multiple sites can be stimulated within a single animal, providing a rich dataset of multiple networks whose organization and mutual relationships can be compared.

Previously, we established that the INS-fMRI method could be used to reveal statistically significant, mesoscale connectivity between subcortical nuclei and cortical areas (Shi et al., 2021; Yao et al., 2023). Our initial study of amygdala stimulation illustrated, via stimulation of a few sites in BA, the feasibility of detecting statistically significant BOLD signal at connected sites in the cingulate cortex and lateral sulcus areas (insular cortex and association sensory areas and auditory belt areas) (Shi et al., 2021). In this study, to understand how different amygdala nuclei mediate brainwide influence, we have systematically acquired, within individual Macaque monkeys, larger datasets of BA, LA, and CeA nucleus stimulation and have evaluated their respective functional connections with cortical areas brainwide. The resulting 'mesoscale functional connectome' of amygdala connectivity (of BA, LA, and CeA) reveals the mesoscale nature of connected sites, the spatial patterns of functional connectivity, and the relative topographic relationships (parallel, sequential, or interdigitating) of nucleus-specific connections. These findings provide novel perspectives on the brainwide circuits modulated by the amygdala, and the intricate interplay of neural circuits involved in various behavioral and emotional processes.

2. Results

Overview. The purpose of this study is to examine the organization of connections between the amygdala and various cortical areas in individual Macaque monkeys. We present our dataset for one monkey (**Figs. 2-5**) and reinforce the findings with consistent data from a second monkey (**Fig. S3**). We note that, compared with most anatomical studies where tracer injections can span several millimeters, our stimulation is significantly more focal, activating a smaller volume of tissue (with intensities used $<1mm^3$ (Cayce et al., 2014)). A major strength of the INS method is that mesoscale networks evoked from multiple sites within an individual can be compared. A weakness is that, due to the focal nature of the stimulation, we are sampling a small volume of the total amygdala. Because INS-fMRI is biased in the 'anterograde' direction, these connections largely reflect amygdalofugal functional connectivity. Our rationale for analysis of the data begins with matrix-based comparison of known anatomy and presence or absence of INS-evoked connections (**Fig. 2E**). Note that, as functional connections include both 'first synapse' and 'second synapse' connections, the functional connectivity networks are expected to be greater than the anatomical connectivity networks. We then examine, within each of the cortical areas (which span limbic, sensory, motor, parietal, and prefrontal cortical areas), the spatial distribution of connections. The examples shown in **Figs. 4 and 5** are selected from matrix zones with strong INS-evoked connectivity (**Fig. 2D**). The brainwide networks of each nucleus are summarized in **Fig. 6**. The mesoscale connectivity topographies revealed are schematically summarized in **Fig. 7**.

2.1 INS of the amygdala reveals remote connections at mesoscale

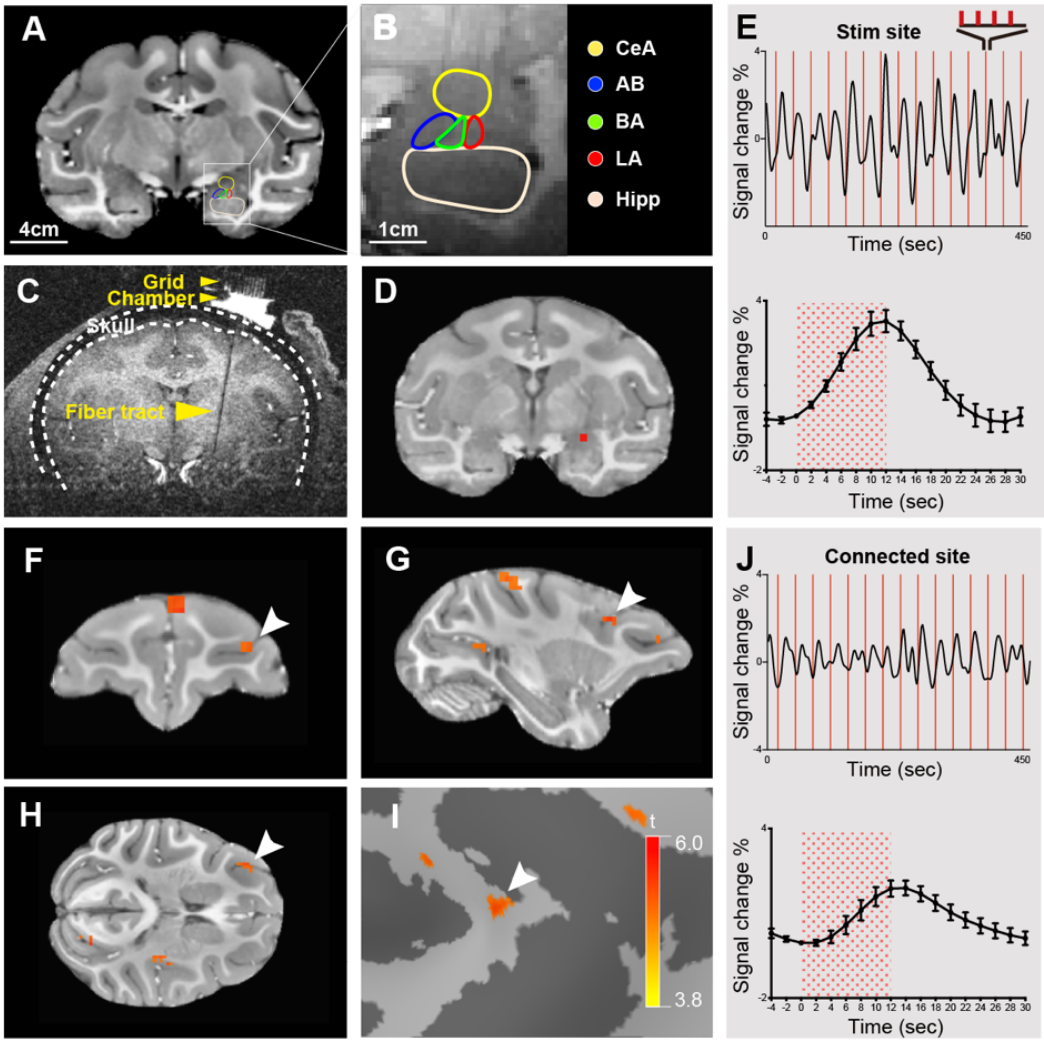

Figure1. Identifying functionally connected sites in the brain following INS stimulation of single mesoscale sites the amygdala. (A) A coronal section through the caudal amygdala. **(B)** Parcellation of the amygdala at the caudal site shown in A. CeA: central amygdala. AB: accessory basal amygdala. BA: basal amygdala. LA: lateral amygdala. Hipp: hippocampus. **(C)** Raw structural image indicating the optical fiber inserted through a grid in a chamber. **(D)** Activation at the laser tip in CeA (red voxel, intensity: 0.2 J/cm^2, $p<1\times10^{-4}$). **(E)** BOLD time course at the laser tip in D. Above: 15 consecutive trials; Below: averaged time course (the dotted rectangle spans the duration of INS). Each red line: one trial of 4 pulse trains (see Methods). **(F-H)** Coronal, sagittal and horizontal view of a remote cluster activated in response to stimulation in D ($p<1\times10^{-3}$). **(I)** Activation cluster (white arrow) in F-H shown on inflated brain surface. **(J)** BOLD time course at connected cluster (white arrow) in F-H. Above: all 15 trials; Below: averaged time course.

To stimulate mesoscale foci in the amygdala, we performed INS stimulation on the right amygdala of a monkey (**Fig. 1A&B**). By inserting a 200μm diameter optical fiber through a preinstalled grid into the amygdala (**Fig. 1C**), we were able to precisely activate mesoscopic sites within the amygdala and determine their nuclear location. For this study,

sites outside of nucleus CeA, BA, or LA were not considered. Periodic trains of infrared neural stimulation at the stimulated site (**Fig. 1D**) evoked BOLD signal response (**Fig. 1E**). As previously shown (Shi et al., 2021; Xu et al., 2019; Yao et al., 2023), functional connectivity at remote sites were evaluated by correlation to the stimulation site (see Methods). **Fig. 1F-I** presents an example of a connected site in the frontal lobe with a timecourse with statistically significant correlation with the INS stimulation (**Fig. 1J**). A correlation value was obtained for every voxel in the brain; only voxels of high statistical significance (T-test $p<1\times10^{-3}$, FDR-corrected $p<2\times10^{-1}$) were further studied. Reproducibility was evaluated using comparisons of half-runs (e.g. even vs odd runs, **Fig. S1**, see also Shi et al 2021). Reliability of activation was also evaluated by examining different thresholds; generally, with lower p-values, activation sizes increased, but activations remained in a similar location (**Fig. S2**, also see (Yao et al., 2023)). In addition, when data from comparable stimulation sites were available from a second animal, we compared these activations; while comparable activations were found (**Fig. S3,** see also (Shi et al., 2021)), differences in detail existed and were attributed to differences in stimulation site location or inter-animal variability.

2.2 Distribution of global cortical connections from CeA, BA and LA

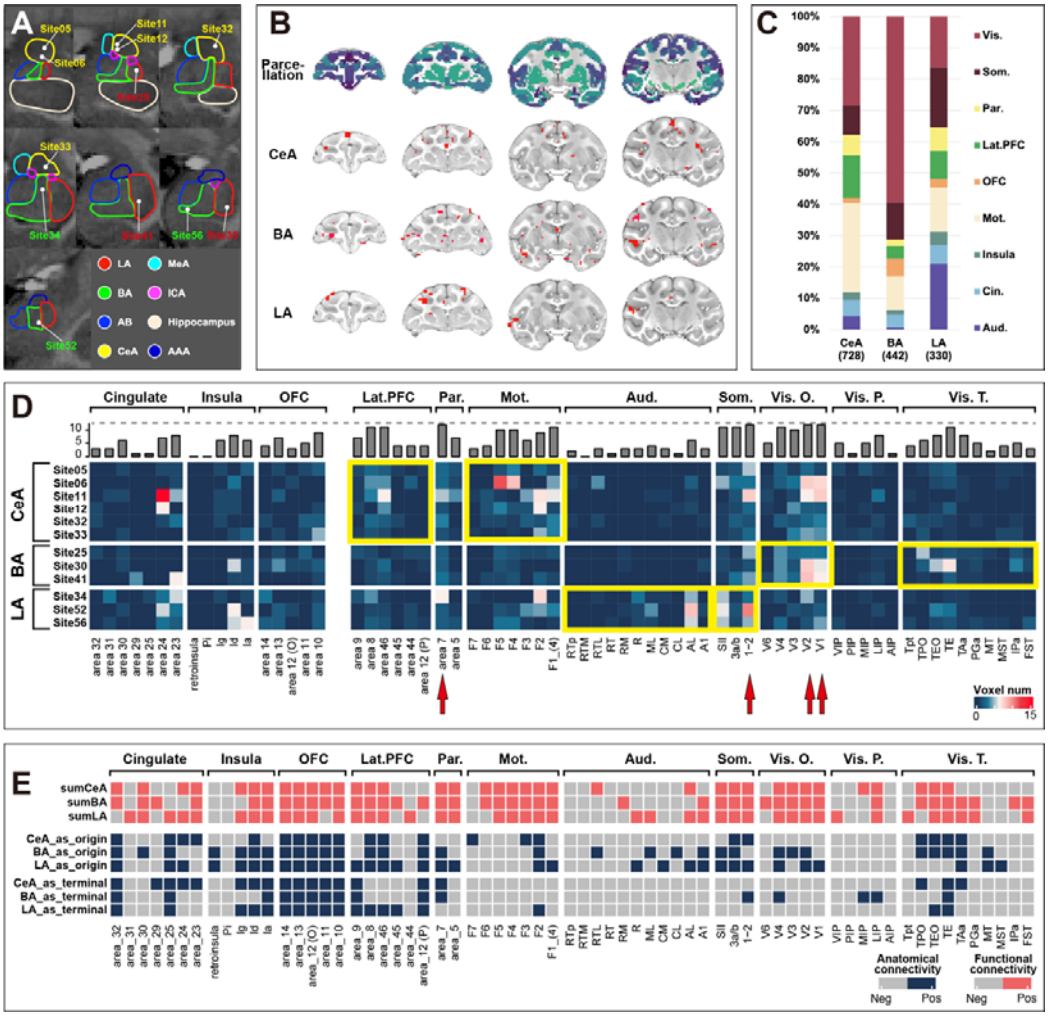

Figure 2 Brainwide connections of the amygdala. (A) The white dots represent the INS stimulation sites in the right amygdala. CeA (yellow contour, 6 sites), BA (green contour, 3 sites), LA (red contour, 3 sites) LA: lateral amygdala. BA: basal amygdala. AB: accessory basal amygdala. CeA: central amygdala. MeA: medial amygdala. ICA: intercalated cell masses. AAA: anterior amygdala area. **(B)** Top row: D99 atlas-based segmentation of brain areas. 2nd-4th rows: examples of significant voxels following stimulation of CeA, BA and LA. **(C)** Proportional composition of cortical connections from CeA, BA and LA (e.g., for all stimulation sites in CeA, the #voxels in an area connected to CeA / total voxels connected to CeA). **(D)** Numbers of voxels activated from CeA, LA and BA ($P<1\times10^{-3}$). The yellow boxes highlight the areas with more robust connections and exemplified in Figs. 4 and 5. The grey bar graph above represents the cumulative number of stimulation sites (total = 12) where connections are present. Red arrows highlight areas activated by all 12 sites in CeA, BA, and LA. **(E)** A comparison of connectivity revealed by INS-fMRI and by anatomical tracers. Upper 3 rows: red represents presence of functional connections. Middle 3 rows: blue represents presence of anatomical connections originating from the amygdala. Lower 3 rows: blue represents presence of anatomical connections to the amygdala originating from the cortex (based on http://cocomac.g-node.org). Vis. T.: visual system (temporal). Vis. P.: visual system (parietal). Vis. O.: visual system (occipital). Som.: somatosensory cortex. Lat-PFC: lateral prefrontal cortex. Par.: parietal cortex. OFC: orbital frontal cortex. Mot.: motor cortex. Aud.: auditory cortex. Pi: parainsula. Ig: granular insula. Id: dysgranular insula. Ia: agranular insula.

To obtain a comparison of amygdala stimulated networks, we examined data acquired within a single animal (6 sites in CeA, 3 sites in BA and 3 sites in LA) (**Fig. 2A**). Note that, unlike anatomical tracer injections which tend to fill more of the amygdala (e.g. a subdivision), this study has sampled very focal (millimeter-sized) locations in different parts of the amygdala. Voxels with significant p-values ($p<1\times10^{-3}$) were selected for subsequent statistical analysis (**Fig. 2B**, see (Shi et al., 2021)). We then examined the brainwide connectivity distributions by calculating, out of the total number evoked from all stimulation sites of each nucleus (CeA: 728, BA: 442, and LA: 330), the percentage of connections associated each different brain area (grouped by function) (**Fig. 2C**). We noted a few distinct characteristics in the three distributions. Relative to BA and LA, CeA had the most functional connections with the motor cortex (28.4%) and the lateral PFC (13.6%). Relative to CeA and LA, BA had the most with the visual cortex (59.6%). And, relative to CeA and BA, LA had the most with the auditory cortex (21.0%) and the somatosensory cortex (19.2%). In contrast, CeA, BA, and LA exhibited similar proportions of functional connectivity with the cingulate cortex (~5%). The differential views of anatomical (literature) and functional (this study) proportional connectivity are likely due to INS revealing (1) additional aspects of networks derived from secondary connections and (2) connectivity patterns arising from mesoscale locations in amygdala.

To further examine the specificity of functional connections, we generated a connectivity matrix between each stimulation site (each row) and each cortical area (each column) (**Fig. 2D**). The results show that CeA exhibits strong connections with motor areas (especially primary F1 and premotor F2 cortex; for one stimulation site, F4 and F5), the PFC (mainly concentrated in frontal eye field areas 8 and 9, and area 46), and with limbic motor cortex (cingulate area 24). These connections may be involved in directing visual attention (eye and head movements) to the socially and emotionally salient

locations the visual field (Gamer and Büchel, 2009; Hoffman et al., 2005; Sander et al., 2005).

Strong connections with visual cortex (especially V1 and V2) and moderately strong connections with somatosensory cortex and area 7 were also seen. The connections of BA with the visual cortex were notably prominent in V2, with strong connections also seen in V1 and somatosensory areas 1 and 2. Some stimulation sites in BA also evoked moderate activation in temporal visual pathway (TPO, TE). Of the three nuclei, auditory areas (primarily belt areas, especially anterolateral belt region, AL) were mostly strongly activated by stimulation of LA, with few connections to core areas (like primary auditory area, A1). Additionally, LA had strong connections with areas 1 and 2 of the primary somatosensory cortex (SI) and the secondary somatosensory cortex (SII) region of the somatosensory cortex; one LA site evoked moderate activations in area 8, area 7, and F2. This thus provides a quantitative view of the prominence of functional connections between focal sites in the amygdala and each cortical area.

Overall, the distribution of functional connections (**Fig. 2E**, upper 3 rows in red) is largely in line with the distribution of anatomical connections. The match appears stronger for the amygdala as 'origin' (**Fig. 2E**, middle 3 rows) than as 'terminal' (that is, anatomical connections to the amygdala originating from the cortex; **Fig. 2E**, lower 3 rows) connections, consistent with previous observations that stimulation evoked connectivity is biased towards 'anterograde' directions. However, there are also substantial differences. The matrix reveals that functional connectivity is present in abundance in some areas where anatomical connections are not prominently observed (such as the motor cortex, somatosensory cortex, and visual cortex), potentially reflecting secondary connections. Another difference lies in the degree of 'common connectivity' of CeA, BA, and LA with single cortical areas. For example, all three subdivisions exhibit extensive bidirectional connections with the OFC. However, anatomical data reveal limited shared connectivity of CeA, BA, and LA with motor cortex, somatosensory cortex, and visual cortex (**Fig. 2D, 2E**). Thus, the functional connectivity data may provide additional views of brain circuitry beyond single synapse networks. Consequently, this suggests that networks of different neuronal clusters within the amygdala may have common functional targets not revealed by anatomical tracing.

2.3 Similarity of functional connectivity and anatomical connectivity in cingulate cortex, insula, and OFC

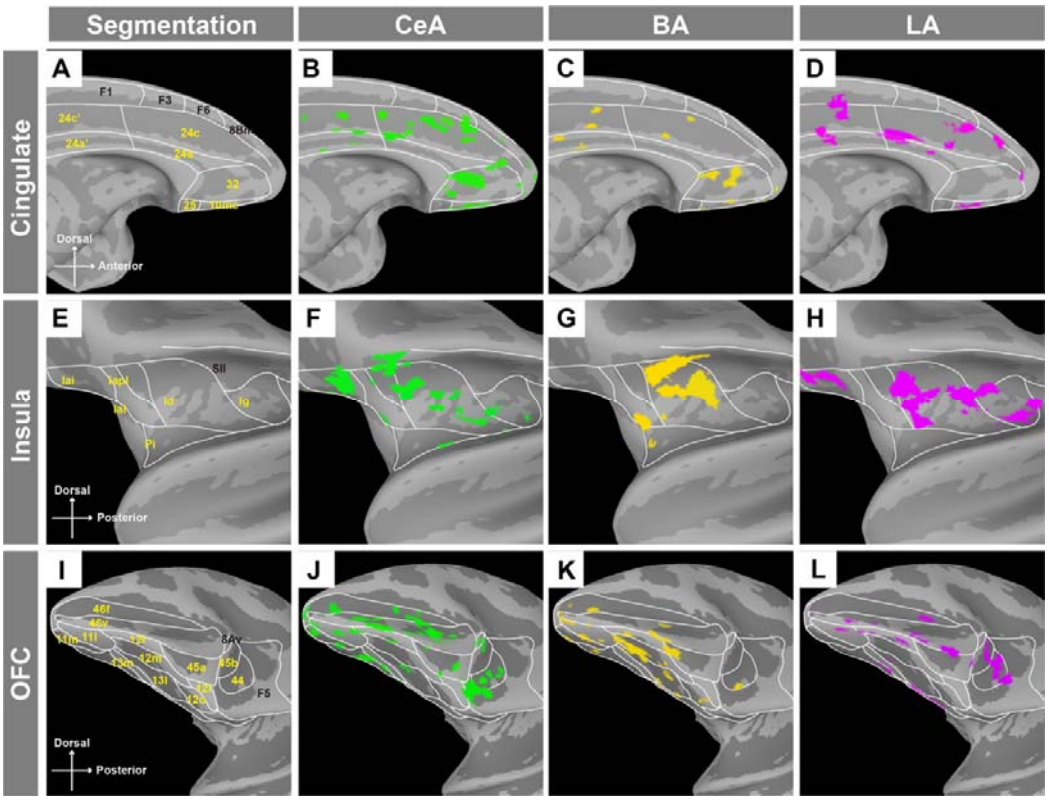

Figure 3 Functional connections with cingulate cortex, insula, and OFC. Topography of connected areas in cingulate cortex (B-D), insula (F-H), and OFC (J-L). Segmentation of the brain areas are shown in the first column (A, E, I). lai: intermediate agranular insula. lapl: posterior lateral agranular insula. lal: lateral agranular insula.

Three of the major cortical connections of amygdala include the cingulate cortex, insula, and the orbitofrontal cortex (Amaral and Price, 1984). Here, we illustrate the connections of all sites from each of CeA, BA, and LA (**Fig. 3B, 3C, 3D**, respectively). The first general observation is that within each of the activated cortical areas, connected sites appear patchy. For CeA stimulations, patchy activations were observed in (1) cingulate areas 23, 24, and 32, and medial orbitofrontal area 10, (2) insular areas in the lateral sulcus (lg, ld, lapl) as well more infra-orbital insular areas lai and lal, (3) lateral prefrontal areas 12, 44, 45, 46, as well as (4) infraorbital areas 11 and 13. BA and LA stimulations lead to similar activation profiles in the cingulate, insular, and PFC (BA activations in cingulate and insula are consistent with previous study (Shi et al., 2021)). Some notable differences include: (1) in contrast to stimulation of CeA and BA, LA shows little activation in area 32 (see also **Fig. 2E**). (2) Stimulation of BA shows little activation in anterior insular area lai or in posterior lg. However, closer inspection reveals that the respective activations of CeA, BA, and LA are largely non-overlapping within each area (**Fig. 3**, see overlay). Overall, while this spatial comparison shows CeA, BA, and LA shares common cortical targets, the mesoscale connectional architecture comprises largely distinct patchy territories within each cortical area, suggesting some degree of functional segregation.

2.4 Mesoscale topographies of areal cortical connections from CeA, BA and LA

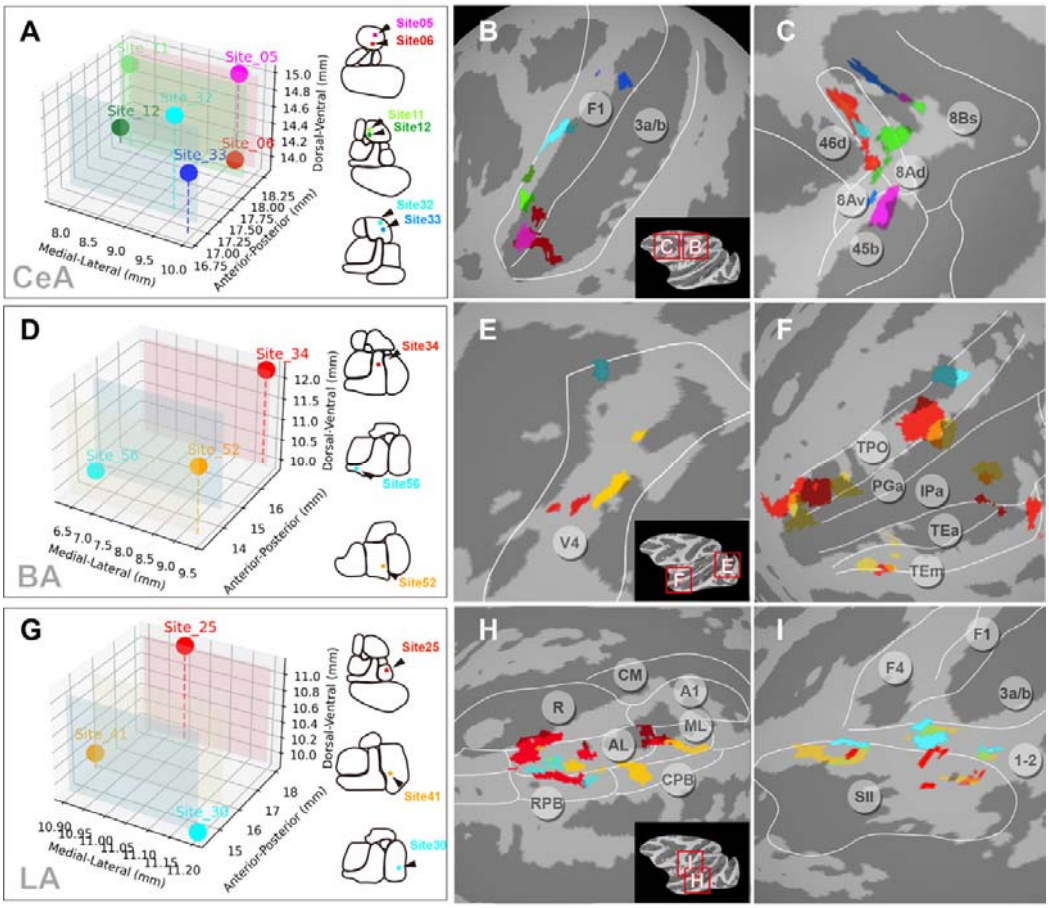

Figure 4 Local cortical topography of connections from the amygdala. Activations from different stimulation sites within each of CeA, BA, and LA were mapped onto the cortical surface ($P<1\times10^{-3}$). (A, D, G) Stimulation sites are shown in 3d coordinates (left) and in rostro-caudal contour cartoons (right). (A-C) Six stimulation sites in CeA revealed connected sites mostly in primary motor cortex F1 (B) and FEF Area 8 (C). (D-F) Three stimulation sites in BA revealed connected sites in area V4 (E) and in ventral visual pathway TP, PG, IP, TE (F). (G-I) Three stimulation sites in LA revealed connected sites in auditory belt areas AL, ML, CPB, RPB (H) and somatosensory areas 1-2 and SII (I). A1: primary auditory area. R: rostral area. CM: caudomedial belt region. AL: anterolateral belt region. ML: middle lateral belt region. RPB: rostral parabelt region. CPB: caudal parabelt region.

We next examined the connections from different stimulation sites within each of CeA, BA, and LA to single cortical areas. These regions were selected based on the presence of activation, for a given cortical area, across multiple stimulation sites (as shown in the matrix in **Fig. 2D**, yellow boxes). As shown in **Fig. 4A**, the six stimulation sites in CeA all led to activations in primary motor cortex (F1) and area 8 of frontal eye field (FEF); these showed distinct and largely non-overlapping topographical distributions. The patches corresponding to the four stimulation sites in posterior parts of CeA (sites 05, 06, 11, and 12) were mainly distributed in the lateral part of the primary motor cortex (**Fig.**

4B), potentially corresponding to the head and face motor areas (Arcaro et al., 2019; Gordon et al., 2023). In contrast, the connections corresponding to the two anterior CeA stimulation sites were located more laterally in primary motor cortex, possibly in the hand motor area. Interestingly, the activations in primary motor cortex arising from the spatially closer stimulation points (Site05 & Site06, Site11 & Site12, Site32 & Site33, each less than 1mm to each other) were also closer to each other on the cortical surface (**Fig. 4B**). For the FEF (**Fig. 4C**), most connection sites were located within area 8Ad and also exhibit little overlap; however, unlike the motor cortex, there appears to be some interdigitation of the activations from CeA anterior (Site05 & Site06) vs CeA posterior sites (Site32 & Site33). In a second monkey, patchy activations were observed in F1 and FEF (**Fig. S3A-C**).

The connections corresponding to the three stimulation sites in the BA (**Fig. 4D**) led to activation of several patches in V4 with the red patches most lateral (foveal), the cyan patch most medial, and the yellow patches intermediate (**Fig. 4E**), suggesting some foveal to parafoveal topography. In the temporal lobe, area TPO contains alternating red and yellow patches anteriorly as well as a single cyan most posterior patch (**Fig. 4E**). Similar, though smaller, red and yellow patches were observed in TE and IPa. In a second monkey, patchy activations were observed in V4 and TPO/IPa (**Fig. S3D-E**).

The connections from the three stimulation sites in LA (**Fig. 4G**) showed both overlapping and interleaved distributions in higher order sensory areas, including auditory belt regions and secondary somatosensory cortex. As shown in **Fig. 4H**, connections in auditory belt cortex were distributed in patchy fashion in AL, with a few additionally distributed in CPB, RPB, and ML. For somatosensory cortex (**Fig. 4I**), the connections are mainly distributed along the border of areas 1-2 and secondary somatosensory cortex, with multiple overlaps in the connections of the three stimulation sites. In a second monkey, patchy activations were observed in auditory (A1, R, AL and somatosensory (SII, 1-2) areas (**Fig. S3G-I**).

In sum, we observed that stimulation of different sites within each of CeA, BA, and LA resulted in patchy activations in connected cortical areas (**Fig. 4,** for the second monkey see **Fig. S3**). Patches were largely distinct and non-overlapping, and exhibited distinct types of topography (e.g., sequential, interdigitating). Data from a second monkey supported the patchy nature of activations. These examples illustrate that the same sites of stimulation within an amygdala nucleus may result in topographic connectivity in one cortical area and interdigitating pattern in another.

2.5 The topography of convergent connections from CeA, BA and LA

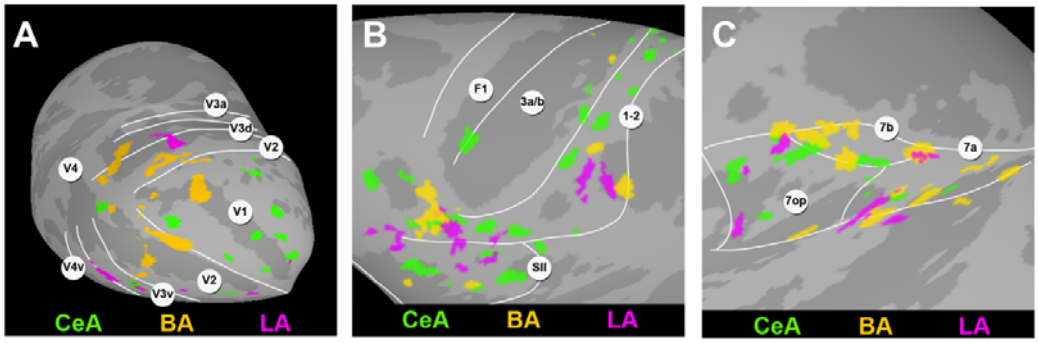

Figure 5 Brain areas with convergent connectivity from CeA, BA and LA. Topography of connected sites in V1/V2 (A), area7 (B), and SI/SII (C), respectively.

We then examined how CeA, BA, and LA connected to the same cortical area. As shown by the matrix of functional connectivity in **Fig. 2D** (red arrows), the brain areas that were strongly activated by all three nuclei include V1/V2, SI/SII, and area 7.

In V1 and V2 (**Fig. 5A**), BA's connections appeared heavily biased towards the foveal region (on the lateral convexity, yellow), connections from CeA were predominantly localized in the peripheral regions (green), and connections from LA were focused in V2, with some connections in V1 and V3 (magenta). Notably, the connections from each nucleus are non-overlapping. In SI/SII (**Fig. 5B**), connections with LA were seen at the border between SI and SII and in the facial sensory area of SI (magenta), while the connections of CeA (green) and BA (yellow) were distributed in areas of SI corresponding to face, hand, and foot. Overlapping patches from LA & BA and from LA & CeA were observed in the face region of area 1-2 and at the border of SI and SII. For area 7 (**Fig. 5C**), the connections from CeA, BA and LA were interleaved and overlapped.

In summary, CeA, BA and LA nuclei all exhibited connections to each of areas V1/V2, SI/SII and area7 in addition to the areas presented above (summarized in **Fig. 6**). The distribution of these connections across the cortex can be described as topographic (shifting), interleaved, or overlapped in organization (**Fig. 7**). Each of V1/V2, SI/SII and area7 exhibits one or more of these connectivity patterns.

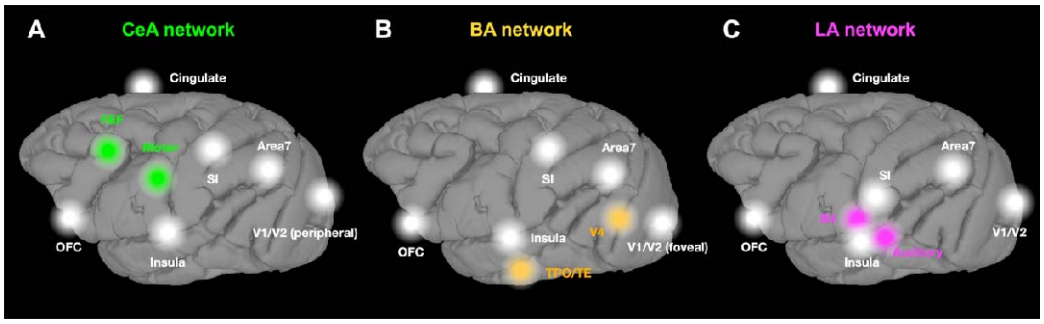

Figure 6 Global networks of CeA, BA and LA. Summarized global networks involving CeA (A), BA (B), and LA (C), respectively. The colored nodes represent divergently connected areas, the white nodes represent convergently connected areas.

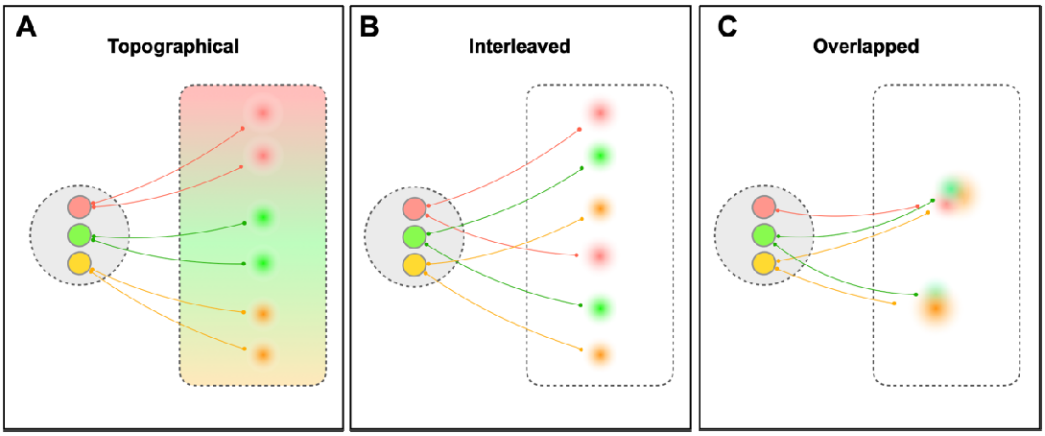

Figure 7 Topographical patterns of connectivity between amygdala sites and brainwide areas. A schematic illustration of connection between the amygdala (left) and the target areas (right).

These findings reveal a mesoscale architecture of brainwide connectivity, where each nucleus of the amygdala relates to functional cortical networks in a systematic (either topographic, interleaved or overlapped) manner. We note that these views of connectional architecture are most clearly revealed when considering locations of high correlation. Lowering the threshold can lead to larger, though still well localized, at millimeters scale, activations centered on the same locations (Yao et al., 2023) (Fig. S2).

3. Discussion

In this study, we used INS to focally stimulate sites within BA, LA, and CeA nuclei of the macaque amygdala. By imaging in a 7T fMRI, we mapped the brainwide cortical connections from each stimulation site. We quantified the distribution and the number of voxels of these cortical connections and summarized them in a matrix. (1) Comparison of the INS connectivity matrix with known anatomical connectivity between the amygdala and cortical areas revealed similarities primarily with 'amygdala as the origin' (**Fig. 2E**), consistent with a the 'anterograde' bias of the INS method (Xu et al., 2019). (2) Our findings showed that activations in cortical connected sites are mesoscale (one to several millimeters) in size and generally these mesoscale patches are non-overlapping (**Figs. 3-5, Fig. S2**). (3) Our findings (**Fig. 4**) showed examples of topographic relationships, where stimulation sites within the same nucleus evoked distinct, shifting patches within target cortical areas. These same sites of stimulation could evoke distinct interleaving patterns of connectivity in other cortical areas. (4) As shown in the matrix, some cortical areas receive inputs from all three CeA, BA, and LA nuclei. Cortical areas with strongest connectivity included the somatosensory cortex, visual cortex, and area 7 of the parietal lobe. Interestingly, the spatial distribution of these connected sites in cortex revealed either differential distribution based on the topographic map (somatosensory cortex SI and visual cortex V1) or an interleaved distribution (area 7).

3.1 Brainwide mapping using INS-fMRI

Using the combination of INS and high-resolution fMRI, we examined the spatial specificity and organization of global networks (**Fig. 6**). While "column-to-column" cortical

connectivity at local scale is known (Hu and Roe, 2022), whether brainwide networks are also so organized is not well established. What is relatively new is the question of what is a 'single' mesoscale node's reach. Hu and Roe (2022) showed that stimulation of a single functional domain (column) in V2 elicits a pattern of intra-areal and inter-areal columns that is repeated across different functional modalities in V2; this demonstrated a minimal (~12 columns) size columnar microcircuit that serves distinct feature modalities. However, whether such brainwide networks are also organizaed in such mesoscale and minimal way has not been studied. Here, our data suggest the presence of analogous minimal mesoscale circuits. Although the amygdala is not organized into columns, local field potentials recorded from single nuclei of the amygdala reveal the presence of neural clusters within amygdala that differentially process visual, auditory, and tactile stimuli (Morrow et al., 2019). This type of mesoscale-to-mesoscale specificity at global scale is still a relatively new concept (Shi et al., 2021).

This study contributes to added understanding of the directional and single- or multi-synaptic aspects of connectivity revealed by a single stimulation site. Previous studies have shown that INS-fMRI is biased towards revealing 'anterograde' activations; that is, stimulation of a single cortical node leads to activation of middle layers in anatomically known feedforward connections and activation of superficial and deep layers in known feedback connections (Xu et al., 2019) (Friedman et al., 2020). Consistent with the 'anterograde' interpretation, our method reveals a better match to anatomical data with amygdala as the origin than as a recipient of cortical inputs (see matrix in **Fig. 2E**). Specifically, anatomical methods reveal projections from amygdala to V2, but not from V2 to amygdala (refs). Our stimulations also replicate this finding: stimulation of amygdala produces robust V2 activation, but there is an absence of activation in amygdala following stimulation of V2 (data not shown: 23 sites, 20 trials per site, no amygdala voxels). This suggests that the connections from CeA to V2 might be disynaptic, possibly through pulvinar or SC or another cortical area such as V1 (Rafal et al., 2015; Weller et al., 2002).

This demonstrates that the study of brain connectivity can extend to include second synapse connections (Huang et al., 2021; Morikawa et al., 2021), providing visualization of larger brainwide networks without the use of trans-synaptic viral tracers.

3.2 The mesoscale architecture underlying multimodal processing networks

We find the functional activations induced by INS stimulation are largely non-overlapping. We bear in mind that our functional activations reveal only the foci of strong connectivity and that there may be functionally connected cells whose connectivity do not reach statistical significance with this method. Given this caveat, our data suggests that amygdala outputs to cortical areas are received in distinct mesoscale regions and that these regions can be arrayed in different topographic patterns (**Fig. 7**). These patchy connections bring into focus distinctions that may not be apparent from traditional anatomical tracer injection studies (Livingstone and Hubel, 1984; Sincich and Horton, 2005), but have been long indicated by anterograde single axon tracing studies (Anderson et al., 2011; Gao et al., 2022; Garraghty and Sur, 1990; Rockland, 2020). This functional stimulation approach offers a way to study and compare the distribution of

multiple connectivity sources. While we do not understand the significance of distinct connectional modes, parallels from studies in the visual system may be informative.

For areas that appear to receive inputs predominantly from one of the three amygdala nuclei (**Fig. 5A**), it could suggest the influence of a single functional domain within the amygdala on the native mesoscale architecture of the recipient cortical area. Although the amygdala has many functional domains that are partially overlapping and hard to dissociate, autonomic and homeostatic control is strongly associated with the CeA. It is possible to envision CeA mediated coupling of certain motor behaviors with autonomic changes, (e.g., the production of facial expressions and other social signals through gestures, postures, etc.) (**Fig. 4B**). Likewise, the connections of the BA and LA that project in an interdigitating fashion to temporal areas, may impact distinct object-based (e.g. face patches) or sensory-based modalities in ventral visual pathway (TPO/TE/V4) and sensory cortex (auditory belt areas, somatosensory areas 1-2/SII), respectively (**Fig. 4E&F, H**). Alternatively, for other areas that receive inputs from multiple nuclei, such as early visual cortex, central visual fields may be dominated by Basal, while extrafoveal regions by CeA influences (**Fig. 5A**) or by integration of the amygdala inputs in face vs. body areas (**Fig. 5B**). Areas such as parietal Area 7 exhibit a highly interdigitating pattern of CeA, BA, and LA inputs, potentially indicating a high degree of limbic, cognitive, and sensory integration for modulating spatial transformations of behavioral maps (**Fig. 5C**). These several patterns of connectivity suggest that amygdala's influence on brainwide networks is mediated in an organized functionally specific manner.

These findings align with our current understanding of cortical function in the following ways: 1) There is spatial topography regarding cortical functions. We know that the cortex contains small functional units, such as cortical columns in the visual cortex (Hubel and Wiesel, 1977) or stripes distributed across the motor cortex (Qi et al., 2010). There is also evidence that within motor cortex the topography for motor action interdigitates with regions for combining action and physiological functions such as arousal and pain (Gordon et al., 2023). Neurons aggregated in the same cortical functional domain share a functional processing goal (e.g., color, shape, disparity, motion in visual cortex, action vs interoceptive nodes in motor cortex, object vs face patches in temporal cortex). Thus, the connections of the amygdala to different units may indicate the amygdala's processing of various features through different internal neuronal clusters. 2) There is integration of multiple sensory and motor functions. Such integration might occur within the functional cortical areas, or in higher-order cortices, or in subcortical structures. Each stimulation site we targeted is connected to multiple cortical areas representing the different axes of behavior, indicating the amygdala plays a significant bridging and integrative role in the emotion-cognitive-sensation-motor circuit.

Taking a step further, we suggest that the mesoscale networks comprise a scaffold upon which dynamic modulation is conducted. That is, within each node are related neurons which share common targets. For example, viral barcode analysis of amygdala-prefrontal connectivity has shown that single amygdala BLA neurons can connect with one to several neurons in different parts of prefrontal cortex (Zeisler et al., 2023). This raises a potential scenario in which dynamics of mesoscale nodal selection is further

coupled with intra-node single neuron selection to achieve a broad range of distinct and specific functional circuits. In this manner, highly organized and sparse mesoscale networks may still achieve a rich repertoire of integrative yet specific affective behaviors. Further studies using different intensities of stimulation in controlled behavioral contexts may test this proposal.

3.3 Comparison with previous studies

To understand the connectivity patterns of the amygdala, the earliest and most direct method employed neural tracers to study connections from an anatomical perspective. This approach led to the recognition of the prominent connections between the amygdala and OFC, insula, and anterior cingulate cortex, establishing the structural basis for amygdala connectivity. Building on this foundation, studies employing electrical stimulation and neurochemical modulation have provided further understanding of effective connectivity of the amygdala; these revealed a broader set of functional connections, including those with the posterior cingulate, retrosplenial cortex, parietal cortex, and temporal cortex(Grayson et al., 2016; Sawada et al., 2022). At the whole-brain level, neurochemical modulation of the amygdala via designer receptors exclusively activated by designer drugs (DREADDs) has shown significant impacts on global brain networks (Grayson et al., 2016; Mueller et al., 2023). Research conducted on stereotactic electro-encephalography in epilepsy patients, through direct electrical stimulation, has observed connected areas shared by BA and LA, including OFC, insula, anterior cingulate cortex, and post-central gyrus, revealing temporal and spatial differences in the connectivity patterns of different nuclei (Sawada et al., 2022). Another study (Zhang et al., 2023) applied electrical stimulation in awake epilepsy patients and evaluated the patients' sensations, revealing the integrative role of various nuclei in mediating emotional reactions and sensory functions including visual, auditory, and vestibular sensations. These studies indicated that the modulation of the amygdala affects not only areas directly connected to it but also the activity of secondary regions. Similar to existing anatomical findings, we observed connections between the amygdala and the OFC, insula, and cingulate gyrus; in addition, focal connections with multiple areas, including the somatosensory, auditory, visual, and motor cortices, exhibited distinct topographic mesoscale organizations. These topographies appeared to fall broadly into three classes described as parallel, interdigitating, and convergent. Our study thus echoes and extends previous findings, revealing the fine-scale organization of how different axes of amygdala function (BA, LA, CeA) influence individual cortical areas as well as selectively integrate brainwide circuits for emotion-guided social behavior.

Acknowledgments: Acknowledgments follow the references and notes list but are not numbered. Start with text that acknowledges non-author contributions and then complete each of the sections below as separate paragraphs.

Funding:

STI 2030−Major Projects 2021ZD0200401 (AWR)

the National Natural Science Foundation of China U20A20221(AWR)

the National Natural Science Foundation of China 819611280292 (AWR)

the Key Research and Development Program of Zhejiang Province 2020C03004 (AWR)

MOE Frontier Science Center for Brain Science & Brain-Machine Integration (Zhejiang University) (AWR)

the Fundamental Research Funds for the Central Universities (AWR)

NIH R01MH121706 (KMG)

Author contributions:

An Ping: Performed surgeries, conducted data analysis, made figures, wrote paper, conducted scans, developed data acquisition and analysis methodology.

Jianbao Wang: Conducted scans, developed methodology, developed data acquisition and analysis methodology.

Miguel Ángel García-Cabezas: Wrote paper, review and editing paper.

Lihui Li: Conducted scans, developed data acquisition and analysis methodology.

Jianmin Zhang: Developed data acquisition methodology.

Junming Zhu: Developed data acquisition methodology, supervise project.

Anna Wang Roe: Obtain funding, design experiments, supervise project and analysis, made figures, and wrote paper.

Katalin Gothard: Obtain funding, made figures, wrote paper, review and editing paper.

Competing interests: Authors declare that they have no competing interests.

Data and materials availability: The data to evaluate the conclusions of this study are available within the article and the supplementary materials. Additional data are available on request.

Methods

Methods used here for macaque monkey animal procedures, amygdala INS stimulation, data acquisition and analysis are similar to that described in (Shi et al., 2021).

Macaque monkeys.

Two hemispheres in two Rhesus macaques (*Macaca mulatta*) were used (Monkey K: right amygdala, Monkey M: left amygdala). We have analyzed and present here 12 stimulation sites from 12 sessions from Monkey K (see **Fig. 2A**), and 6 stimulation sites from 6 sessions in Monkey M (see **Fig. S3**).

Animal preparation and surgery.

All procedures were in accordance with the National Institute of Health's Guide for the Care and Use of Laboratory Animal and with the approval of Zhejiang University Institutional Animal Care Committee. In an initial session, high resolution structural and vascular scans were obtained. Sites to be targeted in the amygdala were then planned and, a grid was implanted in over one hemisphere to aid in the systematic targeting of multiple sites in different nuclei of the amygdala. The animals were sedated with ketamine hydrochloride (10 mg/kg)/atropine (0.03 mg/kg) and anesthetized with 1-2% isoflurane; then, the animals were intubated, placed in a custom MR-compatible stereotaxic apparatus, and artificially ventilated. After local infiltration of skin with lidocaine 1%, a small incision was made in the scalp and a small burr hole craniotomy was then performed at one of the grid site locations determined by previous structural scans for targeting CeA, BA, and LA. During the entire procedure the animal's body temperature was maintained at 37.5-38.5 °C with a water blanket. Vital signs (heart rate, SpO_2, end-tidal CO_2, and respiration rate) were continuously monitored. During the scan, monkeys were maintained with sufentanil (2 to 4 µg/kg per hour CRI (continuous rate infusion); induction, 3 µg/kg supplemented with 0.2-0.5% isoflurane). Vital signs (heart rate, SpO_2, end-tidal CO_2, respiration rate, temperature) were continuously monitored. Following data acquisition, the chamber was cleaned and closed, and animals recovered. Single sessions were conducted once every 1-3 weeks. For terminal experiments in monkey K (which lasted 2-3 days), following completion of data collection, the animal was given an overdose of euthanasia agent iv.

INS stimulation paradigm.

To determine the position of the tip within the amygdala, we conducted a structural scan prior to every INS stimulation run, which revealed a dark spot of signal dropout distinct from surrounding tissues (see **Fig. 1C)**. Stimulation sites were further confirmed by location of fiber tip BOLD activation. We applied INS paradigms previously shown to be effective at neuronal activation. As in our previous studies (Shi et al., 2021; Xu et al., 2019; Yao et al., 2023), INS stimulation (see **Fig. 1**), each trial consisted of 4 pulse trains (12 sec) followed by 18 sec to allow the BOLD signal to return to baseline. Each pulse train lasted 0.5 sec (100 pulses, pulse width 250µs, delivered at 200Hz), with 2.5 sec between each of the 3 pulse trains. This quadruple of pulse trains was delivered once every 30 seconds and repeated 15 times (15 trials) for each run, 1 intensity per run (total period of 450 sec). Radiant exposures which were previously shown to be non-damaging (Chernov et al., 2014; Pan et al., 2023) ranged from 0.1-0.5 J/cm^2. For most of the runs, we used the stimulation intensity of 0.2 J/cm^2. The stimulation intensity was consistent during each run. Typically, 2 runs were conducted per site using 0.2 J/cm^2 intensity.

Data acquisition procedure.

Functional images of voxel size 1.5-mm-isotropic were acquired in a 7-Tesla Magnetom MR scanner (Siemens, Erlangen, Germany) with a customized 6-channel receive coil (inner diameter 6-7 cm) with a single-loop transmit coil (inner diameter 18 cm) and a single-shot echo-planar imaging (EPI) sequence (TE 25 ms; TR 2000 ms; matrix size 86 × 72; flip angle 90°). This coil provided improved homogeneity of temporal signal-to-noise ratio (tSNR) over regular surface coils, resulting in images with similar tSNR values (mean tSNR of gray matter ~75). Functional images from opposite phase-encoding

direction were also acquired for correction of image distortion (Andersson et al., 2003). In addition, Magnetization Prepared Rapid Acquisition Gradient-Echo (MPRAGE) sequence was used to get structural images of voxels size 0.3 mm (monkey K) or 0.5mm (monkey M) isotropic.

Detection of significant responses.
Structural and functional images in raw DICOM files from Siemens scanner were converted to NIfTI (Li et al., 2016) and AFNI (Analysis of Functional NeuroImages) format (Cox, 2012). Functional images were preprocessed with correction for slice timing, motion, image distortion and baseline shift. Significant responses were identified in a commonly used generalized linear model (GLM) approach, in which the timecourse of each voxel was regressed on the stimulus predictor (see **Fig. 1**). The stimulus predictor was the convolution between laser onsets and the standard hemodynamic response function. Regression coefficients were subjected to T-tests. Voxels with significant T-test p-values were highlighted on top of the structural images ($p<1\times10^{-3}$). Only voxels with an FDR-corrected (Benjamini-Hochberg) p value under 20% were included in the following analysis. Individual voxel timecourses were extracted from EPI data with AFNI 3dmaskdump. Timecourses of percentage signal change were calculated at each timepoint t_n as: (Signal(t_n)-Signal(t_0)/Signal(t_0). Timecourses were then averaged over repetitions (15 trials) and plotted. Each baseline was estimated with the mean MR signal over full timecourse. The analyses were done with software AFNI (Cox, 2012), Nipype (Gorgolewski et al., 2011), Bash, R (4.0.2) and Python (3.11.6). Out of all the voxels in the brain, only those voxels with statistically significant correlation with the stimulation site are considered. Significant voxels were visualized on skull-stripped structural images using FreeSurfer v6.0.0 software package (https://surfer.nmr.mgh.harvard.edu/).

Tests for Reliability.
To examine whether these significant sites represent reliable functional connections, several analyses were conducted to support the reliability of the activations. (1) *Half and half analysis*: To examine which voxels were reliable, runs were divided into two groups (e.g. even and odd runs) and GLM correlation analyses as described above conducted. Similarity of the activation pattern supported the reliability of response *(*see **Fig. S1***)*. (2) *Stability across thresholds*: Activation maps were examined using different p values (resulting in larger activation sizes with less significant p values). The corresponding activation patterns remain generally stable, reinforcing the reliability of the method functional connectivity between the amygdala and voxels with significant correlation (see **Fig. S2**, Yao et al 2023). (3) *Similarity across animals*: We compared, across animals, activation patterns following stimulation of the same (or very similar) sites in the amygdala (see **Fig. 4, Fig. S3**, Shi et al 2021).

Image alignment.
All structural and functional images were co-registered to the digital version of rhesus monkey atlas with AFNI command 3dAllineate and 3dNwarpApply. We used D99 digital atlas (version 1.2b) (Reveley et al., 2016) for cortical segmentation, and SARM digital atlas (Hartig et al., 2020) for subcortical segmentation. The alignment was then manually examined according to an MR-histology atlas (Saleem and Logothetis, 2012), as well as www.brainmaps.org for subcortical and brainstem sites, annotations of brain regions were then assigned to all voxels in the brain. Stimulation sites were determined in structural images on which the tip of the optic fiber was dark and distinct from tissues (see **Fig. 1C**) and in functional images based on functional activation (see **Fig. 1D**).

Determining Voxel Number.
We counted the number of voxels in the whole brain (including cortex, subcortical, and brainstem areas), determined using a brain mask (automated, then manually reconfirmed), and then determined by AFNI command 3dBrickStat. The number of voxels activated from each stimulation site, at specific thresholds ($p<1\times10^{-3}$), were then determined and percentage out of total voxels calculated. For area-specific voxel

counting, we applied the aligned atlas to acquire the certain number of activated voxels in different areas.

Anatomical connectivity matrix

To obtain anatomical evidence of connections between the amygdala and various brain regions, we utilized the CoCoMac database (http://cocomac.g-node.org) to identify axonal projections originating from or terminating in CeA, BA, and LA of the amygdala. Initially, we retrieved comprehensive lists of synonymous text IDs for CeA (62), BA (120), and LA (61). Our inclusion criteria were restricted to sites located within single nuclei, while we excluded sites encompassing multiple nuclei (for example, 'basolateral' sites were excluded because they involve both BA and LA). Next, we generate lists of axonal projections by setting amygdala sites as the axon origin sites and axon terminal sites, respectively. Finally, we filtered projections that partially or completely overlapped with the targeted area, supporting the existence of such anatomical connections. For comparison with functional connections (**Fig. 2E**), these anatomical connections were manually attributed to corresponding brain regions of the D99 atlas.

Data visualization.

Prism version 8.4.3 for mac, GraphPad Software, La Jolla California USA was used for statistical analysis. Python version 3.11.5, package "matplotlib" (Hunter, 2007), R version 4.0.2, package " ggplot2" were used for data visualization.

4. Supplementary figures

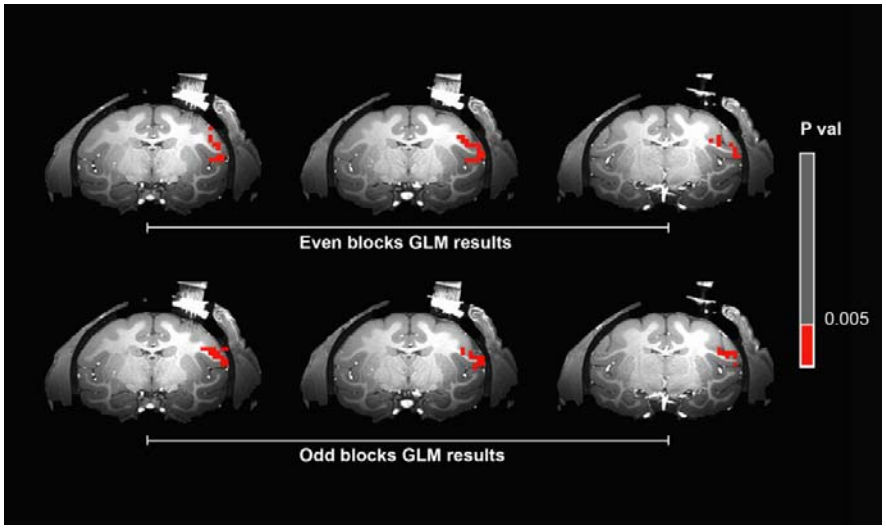

Figure S1 Half and half analysis. To examine which voxels were reliable, trials were divided into two groups (Top: 7 even trials; Bottom: 7 odd trials) and GLM correlation analyses. Voxels are seen in SI (areas 3b, 1) and SII. At the same threshold level for both halves ($p<5\times10^{-3}$), similarity of the activation pattern supports the reliability of response. From Monkey K, Site 12, stimulation in CeA of right hemisphere.

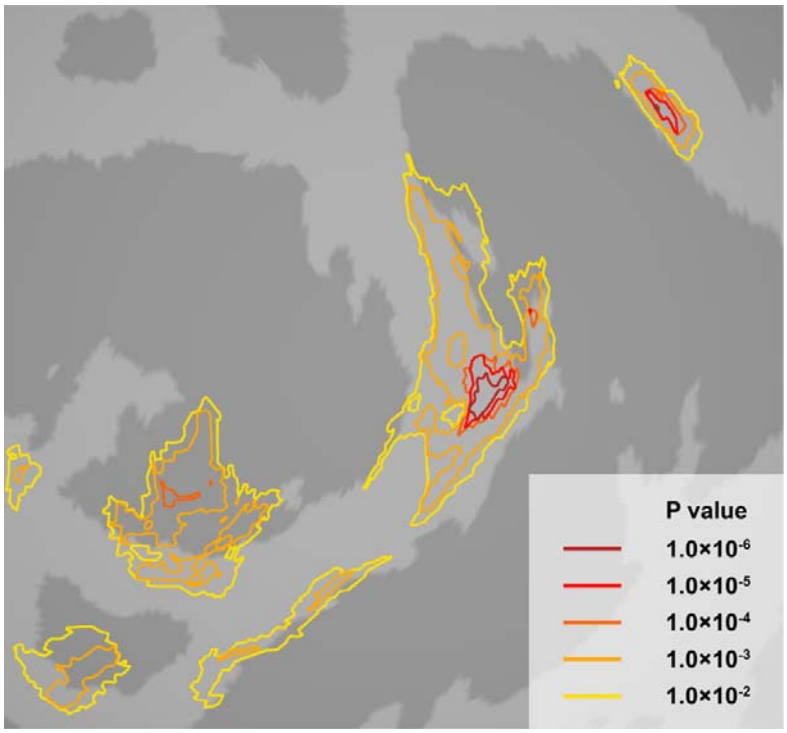

Figure S2 An example of the response patterns at different thresholding p values. The activation evoked by stimulating at a site in medial CeA. The colors of the contours stand for the thresholding percentage. The relationship of thresholds and the

corresponding p values are presented at the right lower corner.

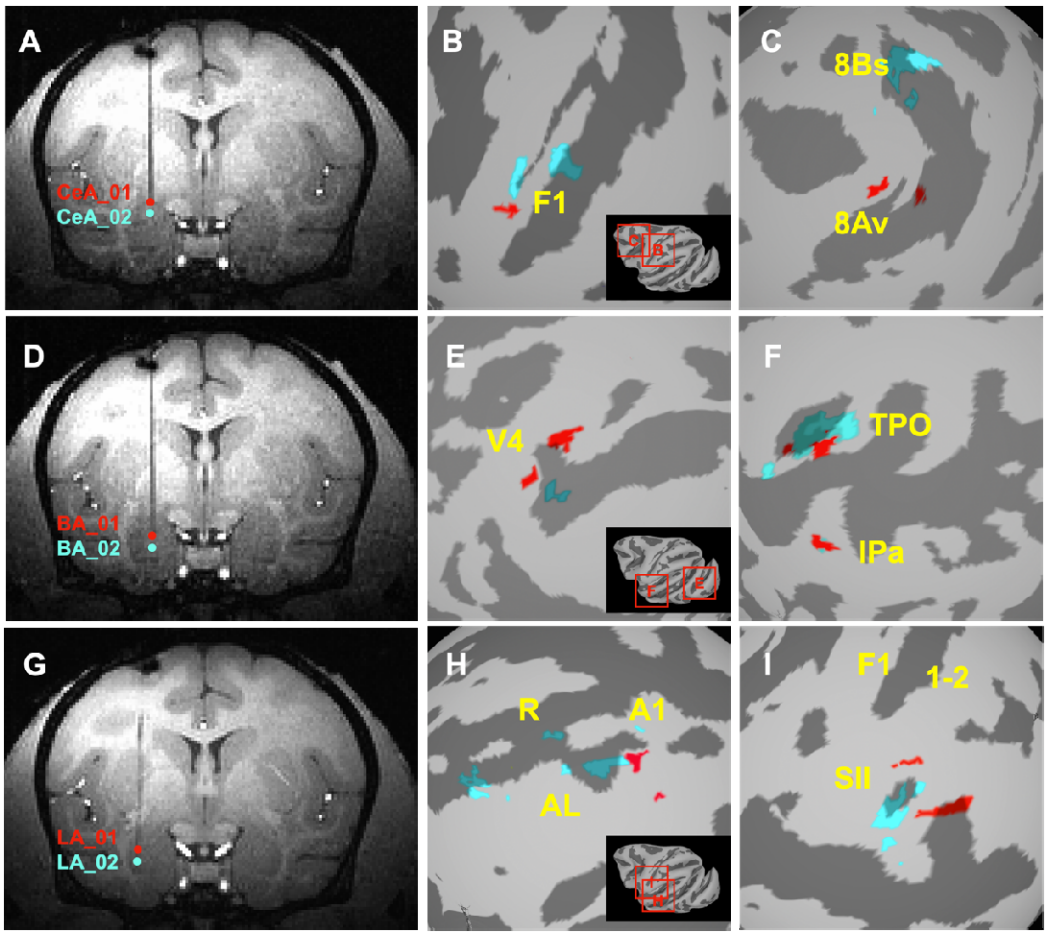

Figure S3 Local cortical topography of connections from the amygdala (Monkey M). (A-C) Two stimulation sites (A) in CeA revealed connected sites in primary motor cortex F1 (B) and FEF Area 8 (C). **(D-F)** Two stimulation sites (D) in BA revealed connected sites in area V4 (E) and in ventral visual pathway TP, IP (F). **(G-I)** Two stimulation sites (G) in LA revealed connected sites in auditory areas (H) and somatosensory areas SII (I). Note that the colored patches ($P<1\times10^{-3}$) indicate activation locations and do not contain correlation strength information. Monkey M dataset: right brain, 17 sites.

Reference

Adolphs, R., and Anderson, D.J. (2018). The Neuroscience of Emotion in Humans. In The Neuroscience of Emotion (Princeton University Press), pp. 251-278.

Amaral, D., and Price, J. (1984). Amygdalo-cortical projections in the monkey (Macaca fascicularis). Journal of Comparative Neurology *230*.

Anderson, J.C., Kennedy, H., and Martin, K.A.C. (2011). Pathways of Attention: Synaptic Relationships of Frontal Eye Field to V4, Lateral Intraparietal Cortex, and Area 46 in Macaque Monkey. The Journal of Neuroscience *31*, 10872-10881.

Andersson, J.L., Skare, S., and Ashburner, J. (2003). How to correct susceptibility distortions in spin-echo echo-planar images: application to diffusion tensor imaging. Neuroimage *20*, 870-888.

Arcaro, M.J., Schade, P.F., and Livingstone, M.S. (2019). Body map proto-organization in newborn macaques. Proc Natl Acad Sci U S A *116*, 24861-24871.

Bickart, K.C., Dickerson, B.C., and Barrett, L.F. (2014). The amygdala as a hub in brain networks that support social life. Neuropsychologia *63*, 235-248.

Cayce, J.M., Bouchard, M.B., Chernov, M.M., Chen, B.R., Grosberg, L.E., Jansen, E.D., Hillman, E.M., and Mahadevan-Jansen, A. (2014). Calcium imaging of infrared-stimulated activity in rodent brain. Cell calcium *55*, 183-190.

Chernov, M., and Roe, A.W. (2014). Infrared neural stimulation: a new stimulation tool for central nervous system applications. Neurophotonics *1*, 011011.

Chernov, M.M., Chen, G., and Roe, A.W. (2014). Histological assessment of thermal damage in the brain following infrared neural stimulation. Brain Stimul *7*, 476-482.

Cox, R.W. (2012). AFNI: what a long strange trip it's been. Neuroimage *62*, 743-747.

Friedman, R.M., Morone, K.A., Gharbawie, O.A., and Roe, A.W. (2020). Mapping mesoscale cortical connectivity in monkey sensorimotor cortex with optical imaging and microstimulation. J Comp Neurol *528*, 3095-3107.

Gamer, M., and Büchel, C. (2009). Amygdala Activation Predicts Gaze toward Fearful Eyes. The Journal of Neuroscience *29*, 9123-9126.

Gao, L., Liu, S., Gou, L., Hu, Y., Liu, Y., Deng, L., Ma, D., Wang, H., Yang, Q., Chen, Z.*, et al.* (2022). Single-neuron projectome of mouse prefrontal cortex. Nat Neurosci *25*, 515-529.

Garraghty, P.E., and Sur, M. (1990). Morphology of single intracellularly stained axons terminating in area 3b of macaque monkeys. J Comp Neurol *294*, 583-593.

Gordon, E.M., Chauvin, R.J., Van, A.N., Rajesh, A., Nielsen, A., Newbold, D.J., Lynch, C.J., Seider, N.A., Krimmel, S.R., Scheidter, K.M.*, et al.* (2023). A somato-cognitive action network alternates with effector regions in motor cortex. Nature *617*, 351-359.

Gorgolewski, K., Burns, C., Madison, C., Clark, D., Halchenko, Y., Waskom, M., and Ghosh, S. (2011). Nipype: A Flexible, Lightweight and Extensible Neuroimaging Data Processing Framework in Python. Front Neuroinform *5*.

Gothard, K.M. (2020). Multidimensional processing in the amygdala. Nat Rev Neurosci *21*, 565-575.

Goyal, V., Rajguru, S., Matic, A.I., Stock, S.R., and Richter, C.-P. (2012). Acute Damage Threshold for Infrared Neural Stimulation of the Cochlea: Functional and Histological Evaluation. The Anatomical Record: Advances in Integrative Anatomy and Evolutionary Biology *295*, 1987-1999.

Grayson, D.S., Bliss-Moreau, E., Machado, C.J., Bennett, J., Shen, K., Grant, K.A., Fair, D.A.,

and Amaral, D.G. (2016). The Rhesus Monkey Connectome Predicts Disrupted Functional Networks Resulting from Pharmacogenetic Inactivation of the Amygdala. Neuron *91*, 453-466.

Hartig, R., Glen, D., Jung, B., Logothetis, N.K., Paxinos, G., Garza-Villarreal, E.A., Messinger, A., and Evrard, H.C. (2020). Subcortical Atlas of the Rhesus Macaque (SARM) for Magnetic Resonance Imaging. bioRxiv, 2020.2009.2016.300053.

Hoffman, L., McDowd, J.M., Atchley, P., and Dubinsky, R. (2005). The role of visual attention in predicting driving impairment in older adults. Psychol Aging *20*, 610-622.

Hu, J.M., and Roe, A.W. (2022). Functionally specific and sparse domain-based micro-networks in monkey V1 and V2. Curr Biol *32*, 2797-2809 e2793.

Huang, L., Chen, Y., Jin, S., Lin, L., Duan, S., Si, K., Gong, W., and Julius Zhu, J. (2021). Organizational principles of amygdalar input-output neuronal circuits. Mol Psychiatry *26*, 7118-7129.

Hubel, D.H., and Wiesel, T.N. (1977). Ferrier lecture - Functional architecture of macaque monkey visual cortex. Proceedings of the Royal Society of London Series B Biological Sciences *198*, 1-59.

Hunter, J.D. (2007). Matplotlib: A 2D Graphics Environment. Computing in Science & Engineering *9*, 90-95.

Janak, P.H., and Tye, K.M. (2015). From circuits to behaviour in the amygdala. Nature *517*, 284-292.

Klein-Flügge, M.C., Jensen, D.E.A., Takagi, Y., Priestley, L., Verhagen, L., Smith, S.M., and Rushworth, M.F.S. (2022). Relationship between nuclei-specific amygdala connectivity and mental health dimensions in humans. Nature Human Behaviour.

Klink, P.C., Dagnino, B., Gariel-Mathis, M.A., and Roelfsema, P.R. (2017). Distinct Feedforward and Feedback Effects of Microstimulation in Visual Cortex Reveal Neural Mechanisms of Texture Segregation. Neuron *95*, 209-220 e203.

LeDoux, J. (2007). The amygdala. Curr Biol *17*, R868-874.

Li, X., Morgan, P.S., Ashburner, J., Smith, J., and Rorden, C. (2016). The first step for neuroimaging data analysis: DICOM to NIfTI conversion. J Neurosci Methods *264*, 47-56.

Livingstone, M.S., and Hubel, D.H. (1984). Anatomy and physiology of a color system in the primate visual cortex. J Neurosci *4*, 309-356.

McHale, A.C., Cho, Y.T., and Fudge, J.L. (2022). Cortical Granularity Shapes the Organization of Afferent Paths to the Amygdala and Its Striatal Targets in Nonhuman Primate. J Neurosci *42*, 1436-1453.

Medina, L., Abellán, A., Morales, L., Pross, A., Metwalli, A.H., González-Alonso, A., Freixes, J., and Desfilis, E. (2023). Evolution and Development of Amygdala Subdivisions: Pallial, Subpallial, and Beyond. Brain Behav Evol *98*, 1-21.

Morikawa, S., Katori, K., Takeuchi, H., and Ikegaya, Y. (2021). Brain-wide mapping of presynaptic inputs to basolateral amygdala neurons. J Comp Neurol *529*, 3062-3075.

Morrow, J., Mosher, C., and Gothard, K. (2019). Multisensory Neurons in the Primate Amygdala. J Neurosci *39*, 3663-3675.

Mueller, S.A.L., Oler, J.A., Roseboom, P.H., Aggarwal, N., Kenwood, M.M., Riedel, M.K., Elam, V.R., Olsen, M.E., DiFilippo, A.H., Christian, B.T.*, et al.* (2023). DREADD-mediated amygdala activation is sufficient to induce anxiety-like responses in young nonhuman primates. bioRxiv.

Pan, L., Ping, A., Schriver, K.E., Roe, A.W., Zhu, J., and Xu, K. (2023). Infrared neural stimulation in human cerebral cortex. Brain Stimul *16*, 418-430.

Pessoa, L., Medina, L., Hof, P.R., and Desfilis, E. (2019). Neural architecture of the vertebrate brain: implications for the interaction between emotion and cognition. Neuroscience & Biobehavioral Reviews *107*, 296-312.

Puelles, L. (2001). Thoughts on the development, structure and evolution of the mammalian and avian telencephalic pallium. Philos Trans R Soc Lond B Biol Sci *356*, 1583-1598.

Qi, H.-X., Jain, N., Collins, C.E., Lyon, D.C., and Kaas, J.H. (2010). Functional organization of motor cortex of adult macaque monkeys is altered by sensory loss in infancy. Proceedings of the National Academy of Sciences *107*, 3192-3197.

Rafal, R.D., Koller, K., Bultitude, J.H., Mullins, P., Ward, R., Mitchell, A.S., and Bell, A.H. (2015). Connectivity between the superior colliculus and the amygdala in humans and macaque monkeys: virtual dissection with probabilistic DTI tractography. J Neurophysiol *114*, 1947-1962.

Reveley, C., Gruslys, A., Ye, F.Q., Glen, D., Samaha, J., E. Russ, B., Saad, Z., K. Seth, A., Leopold, D.A., and Saleem, K.S. (2016). Three-Dimensional Digital Template Atlas of the Macaque Brain. Cerebral Cortex *27*, 4463-4477.

Rockland, K.S. (2020). What we can learn from the complex architecture of single axons. Brain Struct Funct *225*, 1327-1347.

Roe, A.W., Chernov, M.M., Friedman, R.M., and Chen, G. (2015). In Vivo Mapping of Cortical Columnar Networks in the Monkey with Focal Electrical and Optical Stimulation. Front Neuroanat *9*, 135.

Saleem, K.S., and Logothetis, N.K. (2012). A combined MRI and histology atlas of the rhesus monkey brain in stereotaxic coordinates (Academic Press).

Sander, D., Grandjean, D., Pourtois, G., Schwartz, S., Seghier, M.L., Scherer, K.R., and Vuilleumier, P. (2005). Emotion and attention interactions in social cognition: brain regions involved in processing anger prosody. Neuroimage *28*, 848-858.

Sawada, M., Adolphs, R., Dlouhy, B.J., Jenison, R.L., Rhone, A.E., Kovach, C.K., Greenlee, J.D.W., Howard Iii, M.A., and Oya, H. (2022). Mapping effective connectivity of human amygdala subdivisions with intracranial stimulation. Nat Commun *13*, 4909.

Scangos, K.W., Khambhati, A.N., Daly, P.M., Makhoul, G.S., Sugrue, L.P., Zamanian, H., Liu, T.X., Rao, V.R., Sellers, K.K., Dawes, H.E.*, et al.* (2021). Closed-loop neuromodulation in an individual with treatment-resistant depression. Nature Medicine *27*, 1696-1700.

Shapiro, M.G., Homma, K., Villarreal, S., Richter, C.P., and Bezanilla, F. (2012). Infrared light excites cells by changing their electrical capacitance. Nat Commun *3*, 736.

Shi, S., Xu, A.G., Rui, Y.Y., Zhang, X., Romanski, L.M., Gothard, K.M., and Roe, A.W. (2021). Infrared neural stimulation with 7T fMRI: A rapid in vivo method for mapping cortical connections of primate amygdala. Neuroimage *231*, 117818.

Sincich, L.C., and Horton, J.C. (2005). THE CIRCUITRY OF V1 AND V2: Integration of Color, Form, and Motion. Annual Review of Neuroscience *28*, 303-326.

Swanson, L.W., and Petrovich, G.D. (1998). What is the amygdala? Trends Neurosci *21*, 323-331.

Thompson, A.C. (2014). Investigation of infrared neural stimulation in the cochlea.

Weller, R.E., Steele, G.E., and Kaas, J.H. (2002). Pulvinar and other subcortical connections

of dorsolateral visual cortex in monkeys. J Comp Neurol *450*, 215-240.

Xu, A.G., Qian, M., Tian, F., Xu, B., Friedman, R.M., Wang, J., Song, X., Sun, Y., Chernov, M.M., Cayce, J.M., *et al.* (2019). Focal infrared neural stimulation with high-field functional MRI: A rapid way to map mesoscale brain connectomes. Science Advances *5*, eaau7046.

Yao, S., Shi, S., Zhou, Q., Wang, J., Du, X., Takahata, T., and Roe, A.W. (2023). Functional topography of pulvinar–visual cortex networks in macaques revealed by INS–fMRI. Journal of Comparative Neurology *531*, 681-700.

Yu, B., Zhang, Q., Lin, L., Zhou, X., Ma, W., Wen, S., Li, C., Wang, W., Wu, Q., Wang, X., *et al.* (2023). Molecular and cellular evolution of the amygdala across species analyzed by single-nucleus transcriptome profiling. Cell Discov *9*, 19.

Zeisler, Z.R., London, L., Janssen, W.G., Fredericks, J.M., Elorette, C., Fujimoto, A., Zhan, H., Russ, B.E., Clem, R.L., Hof, P.R., *et al.* (2023). High-throughput sequencing of macaque basolateral amygdala projections reveals dissociable connectional motifs with frontal cortex. bioRxiv.

Zhang, H., Wang, D., Wei, P., Fan, X., Yang, Y., An, Y., Dai, Y., Feng, T., Shan, Y., Ren, L., *et al.* (2023). Integrative roles of human amygdala subdivisions: Insight from direct intracerebral stimulations via stereotactic EEG. Hum Brain Mapp *44*, 3610-3623.